ICANS XIX,
19th meeting on Collaboration of Advanced Neutron Sources
March 8 – 12, 2010
Grindelwald, Switzerland

TOTAL DIFFRACTION AND TERMAL DIFFUSE SCATTERING FROM A MULTI-BOUNCE CHANNEL-CUT SINGLE CRYSTAL

J. M. CARPENTER
APS Engineering Support Group
Argonne National Laboratory
9700 S. Cass Aveue
Argonne, Il 60439
and
Neutron Science Division
Oak Ridge National Laboratory
P.O. Box 2008
Oak Ridge, TN 37831

and

M. AGAMALIAN
Neutron Science Division
Oak Ridge National Laboratory
P.O. Box 2008
Oak Ridge, TN 37831

ABSTRACT

We studied Bragg diffraction and Thermal Diffuse Scattering (TDS) from a Si(111) channel-cut triple-bounce crystal using the time-of-flight technique at a pulsed neutron source. Cadmium shielding restricted the detector's direct view of the first bounce surface. The channel-cut crystal dramatically suppresses TDS in the vicinity of the (111), (333) and (444) Bragg reflections; however, TDS appears and increases with the decrease of wavelength in the range of the (555), (777) and (888) orders where cadmium becomes transparent and the single-bounce reflections and TDS contaminate the triple-bounce (555), (777) and (888) reflections.

1. Introduction

U. Bonse and M. Hart [1] introduced channel-cut multi-bounce crystals into diffraction physics more than four decades ago as new optical components of the X-ray Double Crystal Diffractometer (DCD). Theoretically the multi-bounce reflection reduces by many orders of magnitude the tails, or wings, of the Darwin reflectivity function while the resolution and the peak reflectivity is preserved. Originally Si and Ge channel-cut crystals were tested with X-rays [1]. The experimental results appeared satisfactory only for the resolution and the peak reflectivity, but the reflectivity in the wings was many orders of magnitude higher than expected. The dramatic departure from theoretical prediction still is not understood completely and is known in dynamical diffraction physics as the long-standing "wings problem." This parasitic scattering significantly decreases the

sensitivity of DCDs, creating limitations in structural investigations of weakly scattering objects. In spite of this limitation, the Bonse-Hart technique found broad application in small-angle neutron and x-ray scattering (SANS and SAXS) and DCDs on channel-cut crystals are nowadays routinely available at all major synchrotron and neutron laboratories worldwide. Therefore, solution of the wings problem is a subject of great interest for experts in diffraction physics as well as for the large community of scientists using Bonse-Hart DCDs for supra-molecular structural studies of condensed matter.

The Bonse-Hart concept of a "tailless" reflectivity function assumes that the classical Darwin function $R_D(y)$ transforms into $R_D^m(y)$ after m consecutive front-face Bragg reflections inside the channel, which is typically cut from a massive single crystal with diffractive faces parallel to a chosen crystallographic plane. The argument $y = (\theta - \theta_B)/\delta\theta_n$ is the dimensionless angular parameter; $(\theta - \theta_B)$ is the deviation from the Bragg angle θ_B, and $\delta\theta_n$ is the half-width of the Darwin plateau,

$$\delta\theta_n = (\pi V_o \sin 2\theta_B)^{-1} \times [F(h,k,l)\exp(-W)\lambda_n^2]. \quad (1)$$

Meanwhile, the Q-resolution is $\Delta Q = \dfrac{2\pi(2\delta\theta_n)}{\lambda_n}$, so is smaller when λ_n is smaller. In Eq. (1), n is the order of Bragg reflection, λ_n is the wavelength, V_o is the unit cell volume, $\exp(-W)$ is the Debye-Waller factor and $F(h,k,l)$ is the structure factor. In the range of total Bragg reflection $|y| < 1$, $R_D(y) = R_D^m(y) = 1$; however, $R_D^m(y)$ decays according the m power law in the range $|y| > 1$ because in this range

$$R_D(y) = [|y| - (y^2 - 1)^{0.5}]^2 . \quad (2)$$

The Darwin model assumes that the crystal is transparent and infinitely thick; therefore, only the front-face reflection is taken into account. The Ewald function is identical to the Darwin function $R_E(y) = R_D(y) = 1$ when $|y| < 1$; however, because the Ewald theory calculates the total reflection from a transparent, infinitely long crystal of finite thickness $R_E(y)$ becomes different in the range $|y| > 1$,

$$R_E(y) = 1 - (1 - y^{-2})^{0.5} . \quad (3)$$

The relationship between $R_D(y)$ and $R_E(y)$ was established in [2] and can be written as the series of consecutive front- and back-face reflections

$$R_E(y) = R_D(y) + [1 - R_D(y)]^2 \times R_D(y) \times [1 + R_D^2(y) + R_D^4(y) + \ldots] = 2R_D(y)/[1 + R_D(y)], \quad (4)$$

where $R_D(y)$ and $[1 - R_D(y)]^2 \times R_D(y)$ correspond to the first front- and back-face reflections respectively. In the far wings where $R_D(y) << 1$, Eq. 4 can be approximated as

$$R_E(y) \approx 2R_D(y) , \quad (5)$$

reflecting the fact that the first front- and back-face reflections give the same contribution to the wings. Experimentalists can study the $R_D^m(y)$ and $R_E^m(y)$ functions with the DCD by measuring the rocking curves of the analyzer crystal. This technique allows determining parasitic scattering after fitting the experimental results to the theoretical rocking curves, which are calculated as the convolution of the monochromator and analyzer reflectivity functions.

The parasitic scattering from a thick Si triple-bounce channel-cut crystal in the vicinity of Bragg reflections originates from various sources. Usually it is difficult to determine the source of parasitic scattering from only the rocking curve measurements, and thus additional experiments involving modifications of the channel-cut crystal are required.

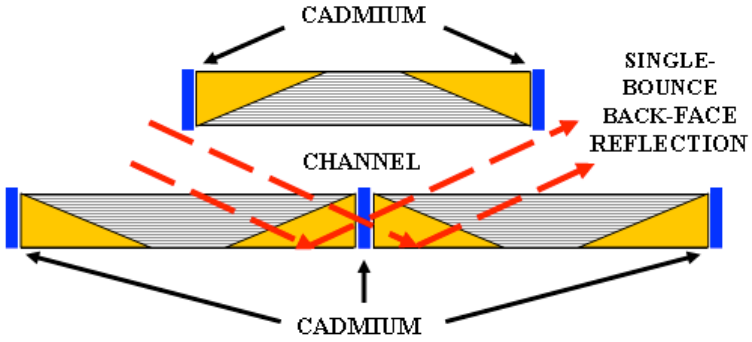

Figure 1. Top view of the channel-cut triple-bounce crystal protected with cadmium plates blocking parasitic single-bounce reflections and edge-face diffraction.

Figure 1 shows the current design of a Si triple-bounce channel-cut crystal, the most applicable in SANS studies, along with the cadmium shielding plates. The yellow triangles indicate the internal areas of diffractive walls blocked for incoming and outgoing neutrons. The neutron beam incident at the Bragg angle can pass the channel only by undergoing triple front- and back-face reflections inside the shaded gray zones. Because Si is nearly transparent for neutrons, the strongest mechanism of parasitic scattering is the admixture of single-bounce back-face reflections [3] passing through the long diffractive wall (see the red dashed arrows in Fig. 1). To eliminate this effect, the original Bonse-Hart channel-cut crystal was modified for application in neutron diffraction by cutting an additional groove in the middle of the long wall and inserting a cadmium plate blocking the parasitic beam propagating in that crystal (see Fig. 1). Also, the edges of the channel-cut crystal are covered by cadmium to eliminate contamination of the triple-bounce reflections by the edge-face diffraction [4]. The surface-induced scattering, as was found in [5], is another parasitic effect, which can be suppressed by polishing and etching the diffractive surfaces of the channel-cut crystal. Nevertheless, in spite of all the described improvements, the experimental reflectivity functions of the Si triple-bounce crystals in the range $|y| > 4$ still show significant departure from the theoretical prediction, reaching several orders of magnitude at $|y| > 12$ [5]. In contrast, excellent agreement of the experimental data with the $R_D^3(y)$ function in the restricted angular range $0 \le |y| \le 4$ was reported in [6].

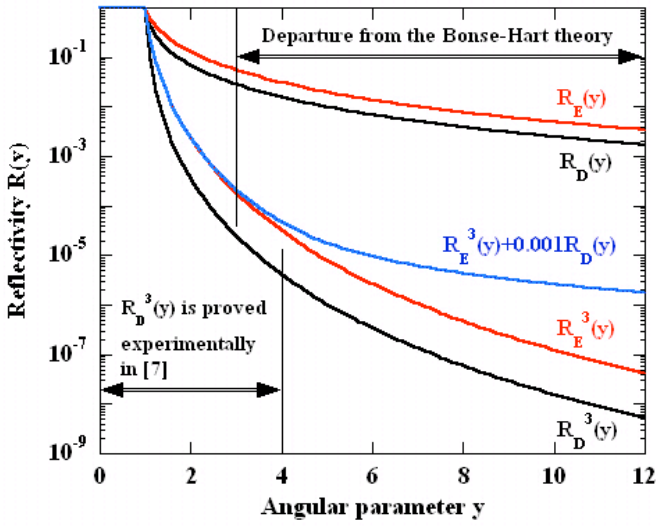

Figure 2. The reflectivity functions $R_D(y), R_E(y), R_D^3(y), R_E^3(y)$ and $[R_E^3(y) + 0.001R_D(y)]$.

Figure 2 summarizes the introductory part of this paper showing the theoretical single- and triple-bounce reflectivity functions $R_D(y), R_E(y), R_D^3(y), R_E^3(y)$ in the range $0 \le |y| \le 12$. Here the departure from the Bonse-Hart model experimentally observed in many studies (see, e.g., in [5, 7]) in the range $|y| > 3$ is simulated with the admixture of 0.1% single-bounce reflection, $0.001\, R_D(y)$, to the cubed Ewald function $R_E^3(y)$. This simple $[R_E^3(y) + 0.001\, R_D(y)]$ model is chosen only to demonstrate the typical y-range and the magnitude of deviation from the theory observed at all the Bonse-Hart DCDs worldwide. This is quite the opposite of the unique experimental proof reported in [6]. That contradiction suggests the existence of additional parasitic effects not discussed yet in this paper: refraction from the edges of Cd plates studied in [8] and thermal diffuse scattering (TDS) from thick Si crystals [9]. Because refraction from the edges can be suppressed by changing the rectangular profiles of the Cd plates for curved ones, the most probable mechanism in our opinion is TDS. The hypothesis that TDS is responsible for the wing problem has not been supported by calculations or experimental results so far. The only attempts to prove that TDS is responsible for the departure from the Bonse-Hart theory were made in [10, 11]. In these studies the multi-bounce channel-cut crystals of a DCD were cooled down with ^{4}He to observe reduction of the rocking curve wings. However, the technical difficulties related to this approach did not enable observation of the expected results. Therefore, we decided to use the pulsed-source neutron time-of-flight technique to investigate the connection between TDS and the wings problem.

It is well known from previous studies (see, e.g., [9]) that thick Si crystals generate TDS in the vicinity of Bragg reflections. The contribution of TDS to the integrated intensity of Bragg reflections increases as $I_{TDS}(\lambda) / I_{Bragg}(\lambda) \sim \lambda^{-3}$ [12], suggesting that TDS originating in the vicinity of high-order Bragg reflections should be significantly stronger than that generated near the first Bragg reflection. The Oak Ridge National Laboratory (ORNL) DCD used in [5] was equipped with a Si(111) mosaic pre-monochromator installed at an unfiltered thermal neutron beam. Therefore, high-order Bragg reflections and TDS were present in the neutron beam entering the double-crystal

arrangement. Because it is not possible to reveal this mechanism of parasitic scattering from rocking curve measurements at steady-state reactors, we addressed the problem using the time-of-flight General Purpose Powder Diffractometer (GPPD), at the Intense Pulsed Neutron Source, Argonne National Laboratory.

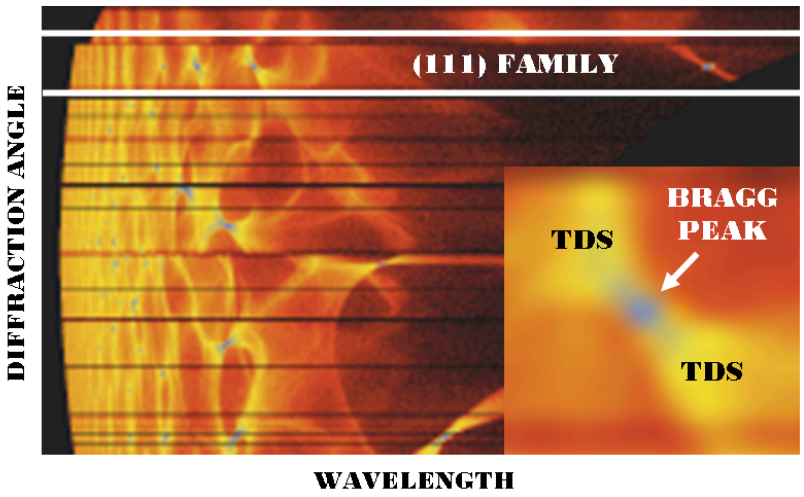

Figure 3. Two-dimensional representation of the GPPD data from a Si(111) slab-shaped single-bounce crystal at $\theta_B = 45°$. The insert shows separately the Si(333) Bragg reflection and nearby TDS.

The first experiment has been run on a slab-shaped single-bounce Si(111) crystal at $\theta_B = 45°$ to test the technique. Figure 3 shows the diffraction data observed for all of the GPPD detectors in the angular range $18° < |2\theta_B| < 156°$ (there are gaps in the angle coverage) as a function of wavelength calculated from the time-of-flight as for elastic scattering. Several families of Bragg reflections appear as tiny bright spots, our particular attention being the (111) family. Surrounding is the scattering that we interpret as TDS, which increases at short wavelength as it should. The intensity distribution displays the periodicity of the Si reciprocal lattice and the phonon dispersion relations, convincingly supporting its origin as TDS.

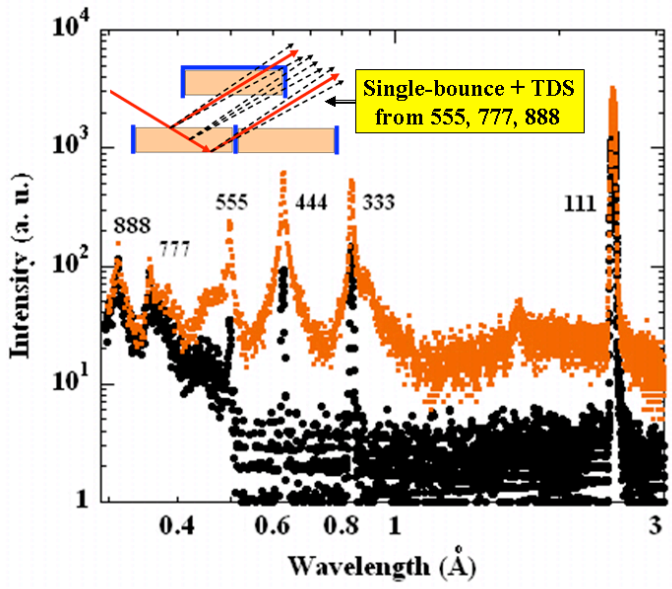

Figure 4. Single-bounce Bragg reflections and TDS (upper curve) from a slab-shaped Si(111) crystal compared with that from the triple-bounce channel-cut Si(111) crystal (lower curve). The insert shows front- and back-face Bragg reflections and TDS emerging from the scattering of non-Bragg-correlated neutrons in the volume. The Bragg angle is 24.4°.

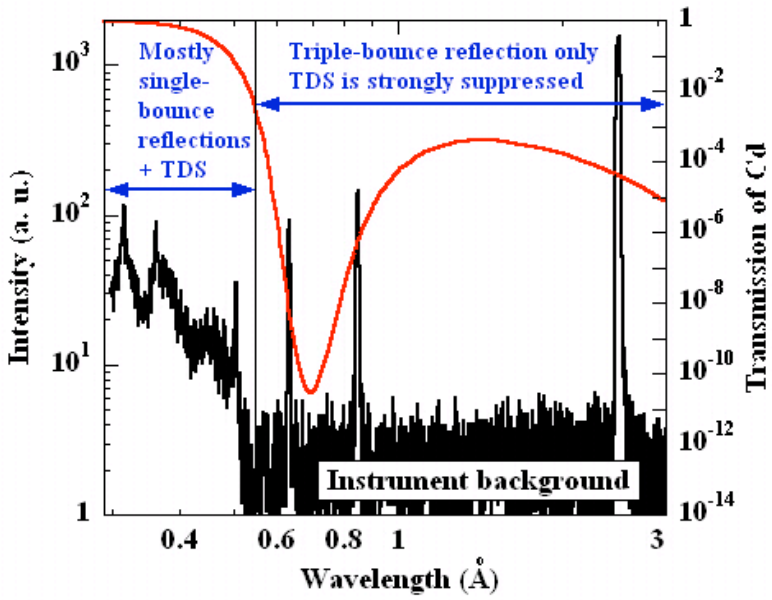

Figure 5. Bragg diffraction and TDS from the Si(111) triple-bounce crystal compared with the transmission of 0.75-mm-thick Cd plate (red line).

The measurements run on the Si(111) channel-cut triple-bounce and the identical single-bounce crystals spanned the wavelength range $0.2 < \lambda < 4.0$ Å. The data collected at three detectors in the angular range $\theta_B = 24.4 \pm 0.75°$ were summed and normalized by the monitor rate and the spectrum of the primary beam. Comparison of the two spectra (see Fig. 4) clearly shows strong suppression of TDS nearby the triple-bounce (111), (333), and

(444) Bragg reflections; however, the reflections (555), (777), and (888) are contaminated with TDS. The spectrum registered from the triple-bounce crystal is presented separately in Fig. 5, highlighting the fact that the increase of TDS in the range of wavelength $0.3 < \lambda < 0.6$ Å correlates with the transmission factor $T_{Cd}(\lambda)$ of 0.75-mm-thick Cd used as the shielding for the Si(111) channel-cut crystal. In the vicinity of the (888) reflection, $T_{Cd}(\lambda) \sim 0.9$, which explains the similarity of the single- and triple-bounce spectra in this range of wavelength. The insert in Fig. 4 demonstrates penetration of (555), (777), and (888) single-bounce front- and back-face reflections and TDS originating along the neutron path inside the crystal wall through the Cd shielding.

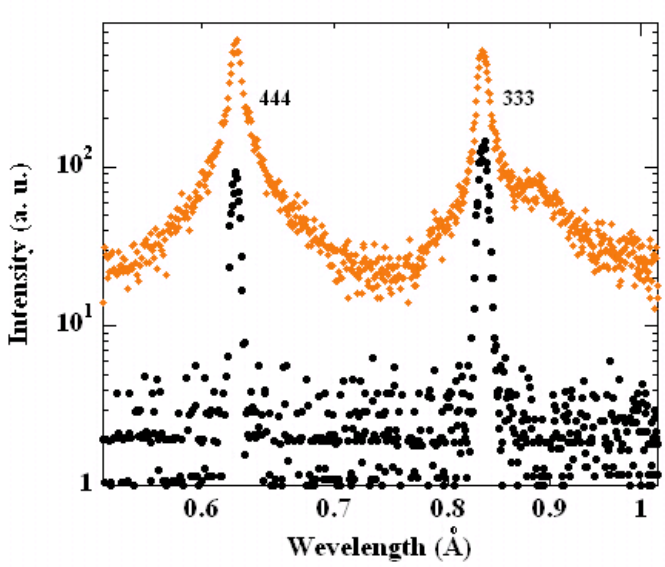

Figure 6. Zoomed view of Figure 4 in the vicinity of the (333) and (444) Bragg reflections.

Figure 6 shows the region including the (333) and (444) reflections on an expanded wavelength scale. Here. TDS severely contaminates the single-bounce Bragg peaks (see the upper curve), while the triple-bounce peaks are free of TDS and what remains nearby is the general instrumental background. Popa and Willis [12] express the integrated intensity of TDS-contaminated Bragg reflections as

$$I_{Total} = I_{Bragg} + I_{TDS} = (1+\alpha) I_{Bragg} \quad , (6)$$

where $\alpha = I_{TDS}/I_{Bragg}$. We integrated our experimental single-bounce data in the range of wavelength $\lambda_B - 0.07\text{Å} \le \lambda \le \lambda_B + 0.07\text{Å}$ and the triple-bounce data in $\lambda_B - 0.018\text{Å} \le \lambda \le \lambda_B + 0.018\text{Å}$, subtracting a linearly interpolated background. Subtracting the triple-bounce intensities from the single-bounce intensities and calculating α_{333} and α_{444}, we found that $\alpha_{333} = 7.0$ and $\alpha_{444} = 14.2$ (a rather large admixture of TDS). Popa and Willis [11, Eq. 3] indicate that α is proportional to λ^{-3}; in our case the experimental ratio $\alpha_{333}/\alpha_{444} = 0.493$, while the ratio of wavelengths $(\lambda_{333}/\lambda_{444})^{-3} = 0.422$. This agreement of the experimental and theoretical α values proves one more time that the observed scattering is indeed TDS.

The time-of-flight experiments illuminate the TDS contribution to the wings of the reflectivity function from Si channel-cut triple-bounce crystal in the range $|y| < 3$ (see Fig. 2). This parasitic effect explains the discrepancy between the results obtained at ORNL [5] and those reported in [6]. The upstream neutron optics of the DCD used in [6] consist of a curved ^{58}Ni neutron guide with the radius $R = 500$ m having the characteristic wavelength $\lambda_c = 5.3$ Å and a PG(002) premonochromator Bragg reflecting $\lambda_1 = 5.24$ Å neutrons to the double-crystal arrangement. This configuration of the upstream neutron optics practically does not transmit the wavelength range $\lambda < 0.6$Å to the Bonse-Hart DCD, and thus the effects described in the present paper could not in principle be observed in [6]. From this point of view the perfect fit to the Bonse-Hart theoretical model reported in [6] supports our conclusion about contamination of the reflectivity function wings with the TDS originating in the vicinity of high-order Bragg reflections with $\lambda < 0.6$Å.

The Time-of-Flight Ultra-Small-Angle Neutron Scattering (TOF-USANS) instrument [13] currently under construction at ORNL's Spallation Neutron Source will incorporate this method of suppressing TDS. The instrument will be equipped with Si(220) channel-cut triple-bounce crystals designed for $\theta_B = 70°$, and thus the first seven orders of Bragg reflection will be in the range $0.5\text{Å} \le \lambda \le 3.6\text{Å}$. Therefore, the first seven triple-bounce Bragg reflections from Si(220) crystals in the TOF-USANS instrument will be protected from contamination by TDS.

Acknowledgements

The authors are grateful to A. D. Stoica for the discussions and fruitful notes and to Ashfiya Huq and Evan R. Maxey for assistance in the measurements. The U. S. Department of Energy supported the work at Argonne National Laboratory under contract number DE-AC02-06CH11357 between Chicago Argonne, LLC and the Department of Energy. This Research for Oak Ridge National Laboratory's Spallation Neutron Source was sponsored by the Scientific User Facilities Division, Office of Basic Energy Sciences U. S. Department of Energy.

References

1. U. Bonse and M. Hart, *Appl. Phys. Lett.* **7**, 238 (1965).
2. T. Takahashi and M. Hashimoto, *Phys. Lett.* A **200**, 73 (1995).
3. M. Agamalian, R. Triolo, and G. D. Wignall, *J. Appl. Crystallogr.* **30**, 345 (1997).
4. C. G. Shull, *Appl. Crystallogr.* **6**, 257 (1973).
5. M. Agamalian *et al.,* J. *Appl. Crystallogr.* **31**, 235 (1998).
6. A. G. Wagh, V. C. Rakhecha and W. Treimer, *PRL.* **87**, 125504-1 (2001).
7. J. G. Barker *et al.*, *J. Appl, Crystallogr.* **38**, 1004 (2005).
8. W. Treimer *et al.*, *Phys. Lett.* A. **305**, 87 (2002)

9. H. A. Graf *et al*., *Acta Cryst*. A **37**, 863 (1981).

10. K. Aizawa and H. Tomimitsu, *JAERI-Review* **2001-005**, 84 (2001).

11. K. Aizawa and H. Tomimitsu, *JAERI-Review* **2002-006**, 107 (2002).

12. N. C. Popa and B. T. M. Willis, *Acta Cryst*. **A53**, 537 (1997).

13. J. M. Carpenter *et al*., J. *Appl*. *Cryst*,, **36**, 763 (2003).